The 8th European Congress on Computational Methods in Applied Sciences and Engineering
ECCOMAS Congress 2022
5 – 9 June 2022, Oslo, Norway

POSTBUCKLING FAILURE MECHANISM OF SQUARE ALUMINUM PLATES UNDER SHEAR LOADING

C. D. KALFOUNTZOS, G. S. E. BIKAKIS AND E. E. THEOTOKOGLOU*

School of Applied Mathematical and Physical Sciences,
Department of Mechanics Laboratory of Testing and Materials,
National Technical University of Athens,
5, Heroes of Polytechniou Avenue, Theochari Bld., Zografou Campus,
GR-157 73, Athens, Greece
*e-mail: stathis@central.ntua.gr, www.ntua.gr

Key words: Shear Panel, Postbuckling, Secondary Buckling, Yielding, Nonlinear Finite Element Analysis.

1 INTRODUCTION

Buckling is very important for structural design, especially when the structure is thin-walled. Slender plates are widely used as structural members in civil, naval and aerospace engineering and they are able to carry considerable additional loads in the postbuckling range. Engineers take advantage of this postbuckling reserve and design structures that are allowed to buckle and operate below their ultimate loads for further weight and cost reduction [1]. Consequently, both buckling and postbuckling behavior of slender plates are of critical importance during the design of lightweight thin-walled engineering structures.

It is known that an elastic flat plate subjected to increasing in-plane compressive loading beyond its primary buckling may snap to another equilibrium state of a different deflection mode. This phenomenon is called secondary buckling of rectangular plates [2].The design of postbuckling structures must include the capability of predicting when secondary buckling occurs, since it is often combined with abrupt mode-shape jump which may give rise to fatigue problems and other degradation factors.

The present numerical study deals with the buckling and postbuckling response of square aluminum simply supported plates subjected to shearing stresses. More specifically, the main objective is the investigation of the failure mechanism of thin plates with different slenderness ratio, taking into account yielding and secondary buckling, which is located using a novel Finite Element Modeling (FEM) procedure.

2 SPECIFICATION OF THE STRUCTURAL PROBLEM

A rectangularsimply supported plate is considered under pure shear. The plate consists of 2024-T3 aluminum and it has length a, width b and thickness t. The analyzed plate is square with a relatively small thicknessand variable slenderness ratio $b/t>$ 106. For the FEM simulation, the plate is subjected to in-plane shear displacement loading along its four edges. More specifically, Multipoint Constraints (MPCs) are used and the controlled shear displacement is applied at the master node of each edge (MN1-MN4), as it is shown in Figure

1. The applied shear displacement is then transferred to all other nodes of each edge which are the slave nodes. The plate will buckle for a critical value of the applied displacement corresponding to a total shear forceN_{XYo}applied at each edge,and it will continue to carry additional load in the postbuckling range. Depending on the slenderness ratio, the simulation is terminated when the plate collapses (due to material yielding) or when its secondary buckling occurs.

The primary buckling isdetermined using the classical eigenvalue buckling analysis of ANSYS FEM software [3], whereas the secondary buckling is predicted with new FEM procedures. Load-deflection amplitude curves will be constructed using nonlinear FEM analysis results in order to predict the postbuckling reserve and the load-carrying capacity of the plates. It is noted that the slenderness ratio of all plates of this research has been selected so that the elastic primary shear buckling precedes yielding.

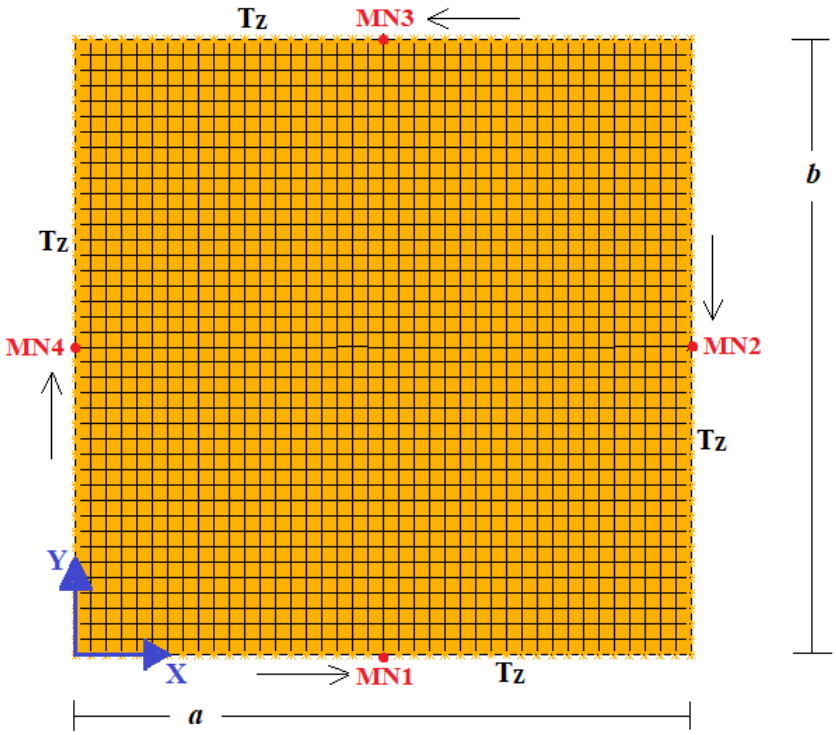

Figure 1: Finite element mesh of a square 0.2 m x 0.2 m plate (a/b = 1) along with the shear displacement loading at the master node of each edge and the simply supported boundary conditions

3 FEM PROCEDURES

The plates of this study aremodeled usingthe four-noded quadrilateral SHELL181 [3] elements, which are suitable for analyzing thin to moderately thick shell structures. The postbuckling failuremechanism of 2024-T3 aluminum square plates is determined by employing the nonlinear analysis of ANSYS,with geometric andmaterial nonlinearities. The von Mises stresses are used to locate the onset of yielding and monitor the spread of plasticity.

The elastoplastic material behavior of 2024-T3 aluminum is modeled using a bilinear

stress-strain relationship with kinematic hardening law. For the definition of this material model it is necessary to specify the Young's modulus E, the Poisson's ratio ν, the yield stress σ_y and the tangent modulus E_t. From reference [4] we have used the following material properties: E = 73.084 GPa, ν = 0.33 and σ_y = 369 MPa. The following relation is used in order to specify E_t [3]:

$$E_p = \frac{E\,E_t}{E-E_t} \tag{1}$$

where E_p is the plastic modulus of aluminum.

Considering that E_p = 1.3 GPa [5] and using Equation (1) the tangent modulusE_t is calculatedequal to 1.277 [GPa].

The simply supported boundary conditions (bc) along the edges of the plate have been applied as shown in Figure 1 with the symbol T_Z which means that the nodal translations are constrained in the out-of-plane Z-direction. The coordinate system is always orientated as shown in Figure 1.

For the prediction of the secondary buckling load it is required to determine the equilibrium path of the shear panel from the beginning of loading up to the point of secondary buckling. The path consists of the first part corresponding tolinear elastic prebuckling stage and the second part corresponding to nonlinear structural behavior. The nonlinear postbuckling stage starts from the point of primary bucklingand continues up to the point of secondary buckling. However, it is possible that the postbuckling behavior of the plate becomes elastoplastic and the plate may even collapse and stop carrying additional load before the secondary buckling, depending on its slenderness ratio.

For the determination of the equilibrium path a nonlinear FEM analysisis needed with an imperfection having the shape of the critical eigenvalue buckling mode shape$\boldsymbol{v_1}$ [6]. In order to locate the secondary buckling point, a novel numerical procedure is proposed. Considering a set of points in the postbuckling range, as moving gradually from the primary buckling point, their equilibrium is perturbed with the application of perturbation loads. Then, in order to locate the position of the secondary instability, the plate's equilibrium is examined using eigenvalue buckling analyses implemented at the specific equilibrium positions.

Initially, an eigenvalue buckling analysis is implemented according to ANSYS recommendations [3], in order to obtain the aforementioned imperfection. The imperfection $\boldsymbol{v}$ is set as a linear equation of the first eigenvector: $\boldsymbol{v} = \omega t\boldsymbol{v_1}$, where $\omega$is set equal to 0.01 [1]. It is noted that the convergence of the critical primary buckling load N_{XYo} and the associated mode shape is always verified by comparisons of results corresponding to fine and very fine plate mesh density. The nonlinear analysis is then implemented using the arc-length method and it is terminated when the imposed shear displacement corresponds to a point in the postbuckling range where the plate's equilibrium will be examined. After the termination of the nonlinear analysis, an eigenvalue analysis is performed using the linear perturbation analysis procedure and it is based on the following equation [3]:

$$[K_T]\{\varphi_j\} - \lambda_j[S_P]\{\varphi_j\} = \{0\} \tag{2}$$

where $[K_T]$ is the total tangent stiffness matrix,

$[S_p]$ is the perturbed stress stiffening matrix,

λ_j and $\{\varphi_j\}$ are the eigenvalues and the eigenvectors, respectively.

Having obtained the lowest critical eigenvalue $\lambda_C$from the solution of Equation (2), the total buckling load $\{F_b\}$ can be calculated as follows:

$$\{F_b\} = \{F_r\} + \lambda_C\{F_P\} \tag{3}$$

where $\{F_r\}$ is the total load at the current point,
$\{F_p\}$is the perturbation load.

It is observed from Equation (3) that when $\lambda_C = 0$, $\{F_b\} = \{F_r\}$, which means that buckling will occur at the specific point. Consequently, the condition $\lambda_C > 0$ means that some additional load (shear displacement) is needed for the buckling of the plate; decreasing values of λ_C corresponding to consecutive nonlinear analyses with increasing shear displacement, which eventually become very small and approach zero, mean that the secondary buckling of the plate is very close to the last considered point of the postbuckling range. In order to ensure that secondary buckling does occur at the predicted point, the predicted secondary buckling compression is slightly increased and new analysis is performed to verify that λ_C becomes negative. A change of sign of λ_C mean that it becomes equal to zero practically at the predicted secondary buckling point.

The convergence of the load-deflection curve of the considered equilibrium path along with the calculated secondary buckling load is always verified by comparison of results corresponding to fine and very fine plate mesh density.

The secondary shear buckling coefficient of monolithic aluminum plates is calculated by [2, 7]:

$$k = \frac{N_{XYc}b}{\pi^2 D} \tag{4}$$

where D is the bending stiffness of the isotropic plate and N_{XYc} is the secondary buckling shear force.

Equation (4) can also be used to calculate the primary shear buckling coefficient k_o; the only change is N_{XYc} being replaced by N_{XYo}.

FEM models with three different values of slenderness ratio (b/t) are built, in order to examine the failure mechanism of square aluminum plates under shear loading. More specifically, the thickness t of the plates is constant and equal to 1.875 mm. The dimension $b = a$ varies so that the slenderness ratio is equal to 106.7, 213.3 and 426.7.

4 COMPARISON OF FEM RESULTS WITH LITERATURE RESULTS

We have carried out suitable comparisons between the FEM results and corresponding literature results for monolithic aluminum rectangular plates in order to validate our FEM models.

Initially, we have compared the FEM results with corresponding analytical results obtained from a solution concerning symmetric and antisymmetric buckle patterns of simply supported rectangular flat plates in shear [8]. An excellent agreement between the FEM values and the analytical values of the primary shear buckling coefficient k_o can be observed from Table 1, since their deviation is very small. The symbol m represents the number of large buckles of the plate corresponding to the primary buckling mode shape. It is noted that a very good agreement is also found between the FEM calculated mode shapes and the mode shapes presented in [8]. These facts demonstrate the validity of the implemented numerical procedure

for the calculation of the primary shear buckling load and mode shape. The applied bc and shear displacement loading using MPCs are also validated.

Table 1: FEM versus analytical [8] values of primary shear buckling coefficients of aluminum rectangular plates with simply supported bc under pure shear

a/b	*m*	k_o, analytical [8]	k_o, FEM	k_o deviation (%)
1.0	1	9.35	9.33	-0.21
1.2	1	8.00	7.99	-0.13
1.5	1	7.07	7.08	+0.14
2.5	2	6.06	6.04	-0.33
3.0	2	5.89	5.85	-0.68

We now following the reasoning reference [9]. Having validated our FEM models for the primary shear buckling, the nonlinear analysis of ANSYS is performed as described in section 3 of this article using the validated models to assess the postbuckling behavior of the shear panels.

In order to validate the novel FEM procedure with respect to the secondary buckling load calculation described in the previous section we have compared the numerical results with corresponding theoretical results [2] for isotropic simply supported plates under uniaxial compression,since there are not any published pertinent results concerning the secondary shear buckling of plates. It is noted that the novel FEM procedure does not depend on the geometry, the loading and the bc of the structure. An excellent agreement can be observed between our FEM results and the analytical predictions of secondary buckling coefficient k_c from Table 2. Additionally, the numbers of longitudinal half-waves of the FEM buckled mode shapes agree with analytical predictions of [2]. It is noted that the symbol $\overline{K}$ in Table 2 represents the non-dimensional spring stiffness coefficient of an elastic spring support as it is defined in [2]. Consequently, the validity of the implemented numerical procedure for the calculation of secondary buckling load is demonstrated from these comparisons. The applied bc and compressive loading are also validated.

Table 2:FEM versus analytical [2] values of secondary buckling coefficients of isotropic rectangular plates (ν=0.3) with simply supported bc under uniform axial compression

a/b	$\overline{K}$	k_c, analytical [2]	k_c, FEM	k_c deviation (%)
5.0752	0	12.3890	12.5148	+1.015
4.8926	∞	3.7614	3.7958	+0.915
2.4480	0	6.4800	6.4781	-0.029
3.9400	∞	5.3100	5.3654	+1.043

The FEM calculated secondary buckling load is compared with Stein's experiment [10] and a very good agreement is also found. The secondary buckling coefficient reported in Stein's experiment, for an isotropic aluminum (ν=0.33) plate with clamped loaded edges and aspect ratio *a/b*=5.384, is k_{Stein}=7.36, whereas the one calculated using ANSYS is k_{FEM}=8.019 (+8.95% deviation).

5 RESULTS AND DISCUSSION

The maximum out-of-plane deflection w_{max} of the buckled square plate with symmetric buckle pattern is located at its center andit can be used to analyze the postbuckling out-of-plane deformation of the plate. In Figure 2 the (N_{XY}, w_{max}) curves ofsquare 2024-T3 aluminum plates are depicted for variable slenderness ratio. Depending on the *b/t* value, the curves of Figure 2 stop either at the predicted point of secondary buckling or at the point of collapse.More specifically, in the case of the thickest plate (*b/t*=106.7) the first part of the curve corresponds to the elastic prebuckling stage and it is shown that as the loading increases w_{max} remains null up to the point of primary buckling, where the out-of-plane deflections start to increase as well. The next part of the curvecorresponds to the elastic postbuckling stage, in which the behavior of the plate becomes geometrically nonlinear. This elastic postbuckling stage starts from the point of primary buckling and is ended when the onset of yielding occurs forw_{max}=3.87 mm (Figure 2).Afterwards, plasticity spreads until one complete narrow diagonal yield line is formed which causes the collapse of the plate [9]. This finding can be observed graphically from Figure 2 since the tangent to the curve of the plate with *b/t*=106.7 becomes parallel to the horizontal axis at the end of the postbuckling path indicating the collapse. Consequently, the onset of yielding and the failure of the plate precede the secondary buckling for the case with the lowest slenderness ratio.

Although the curve of Figure 2 corresponding to *b/t*=213.3 is similar to the curve described in the previous paragraph, it stops at the predicted point of secondary buckling.In this case of slenderness ratio,the secondary bifurcation precedes the collapse of the plate. More specifically, the elastic postbuckling stage now occupies a larger part of the postbuckling pathsince the onset of yield is observed for w_{max}=8.57 mm. As a result, although the elastoplastic response of the plate begins from this point, the secondary buckling occurs before the collapse of the plate due to material yielding.

The entire postbuckling path of the more slender plate (*b/t*=426.7) is elastic and the corresponding curve of Figure 2 stops at thepredicted point of secondary buckling.

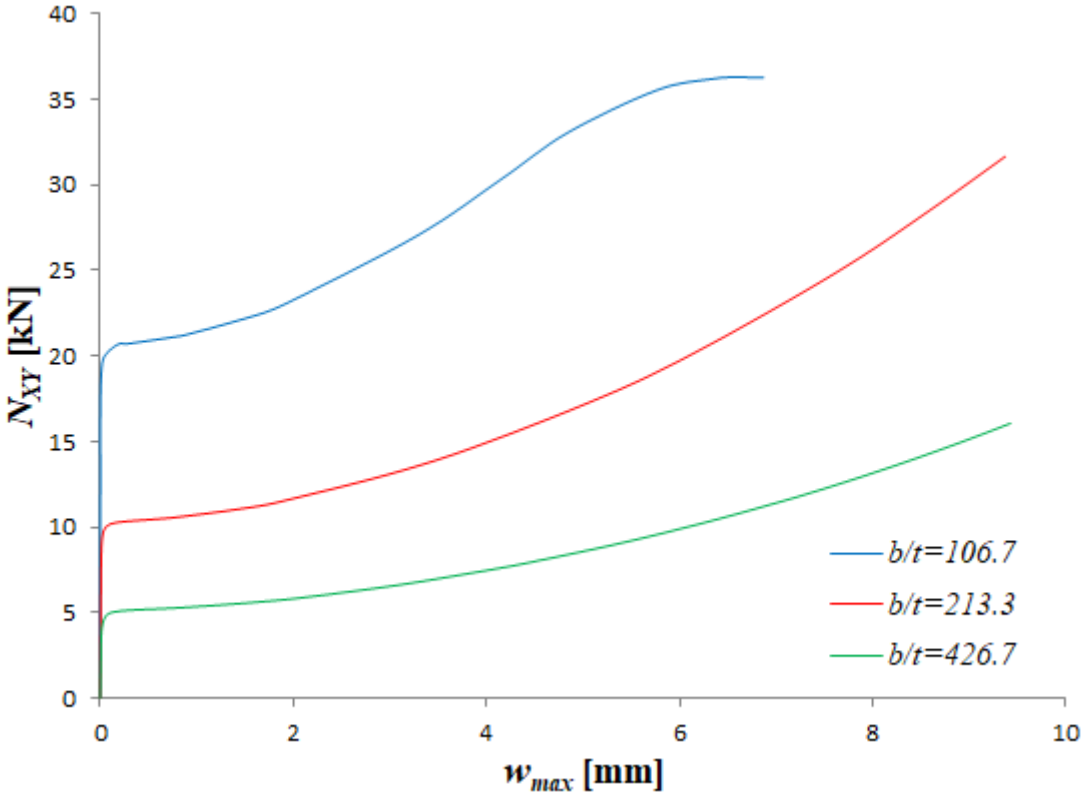

Figure 2: FEMshear force versus maximum out-of-plane deflection of aluminum square plates under pure shear with different slenderness ratios

It is obvious from Figure 2 that the position of the primary buckling point (which is located near the intersection of the prebuckling and postbuckling branches) and the corresponding buckling load are strongly affected by the slenderness ratio of the plate. As *b/t* decreases the primary buckling load is increased. It is shown from Figure 2 that the position of the secondary buckling point and the corresponding secondary buckling load are also strongly affected by the slenderness ratio of the plate. As *b/t* decreases the secondary buckling load is increased.

It is concluded from the previous discussion that variations of the slenderness ratio can alter the order of first occurrence of the following phenomena as the loading increases: onset of yielding, secondary buckling, collapse of the shear panels.Additionally, it is found that as the plate becomes more slender, the secondary buckling precedes the onset of yielding.

In Figure 3 (a) the von Mises stress contours at the top and bottom external surfaces are depicted for thethickest square aluminum plate (*b/t* = 106.7) at the end of its postbuckling path. It has been verified during the postprocessing of FEM results that plasticity has spread at both external surfaces of the plate (within the depicted red color areas). Furthermore, a diagonal yield line has been formed which causes the collapse of the plate. In Figure 3 (b) the postbuckling deformation mode of the same plate is depicted using contour plot of the out-of-plane deflectionscorresponding to the point ofcollapse of the plate. In this figure the formation of one symmetric large buckle is observed with the maximum out-of-plane deflection located at the center of the plate.

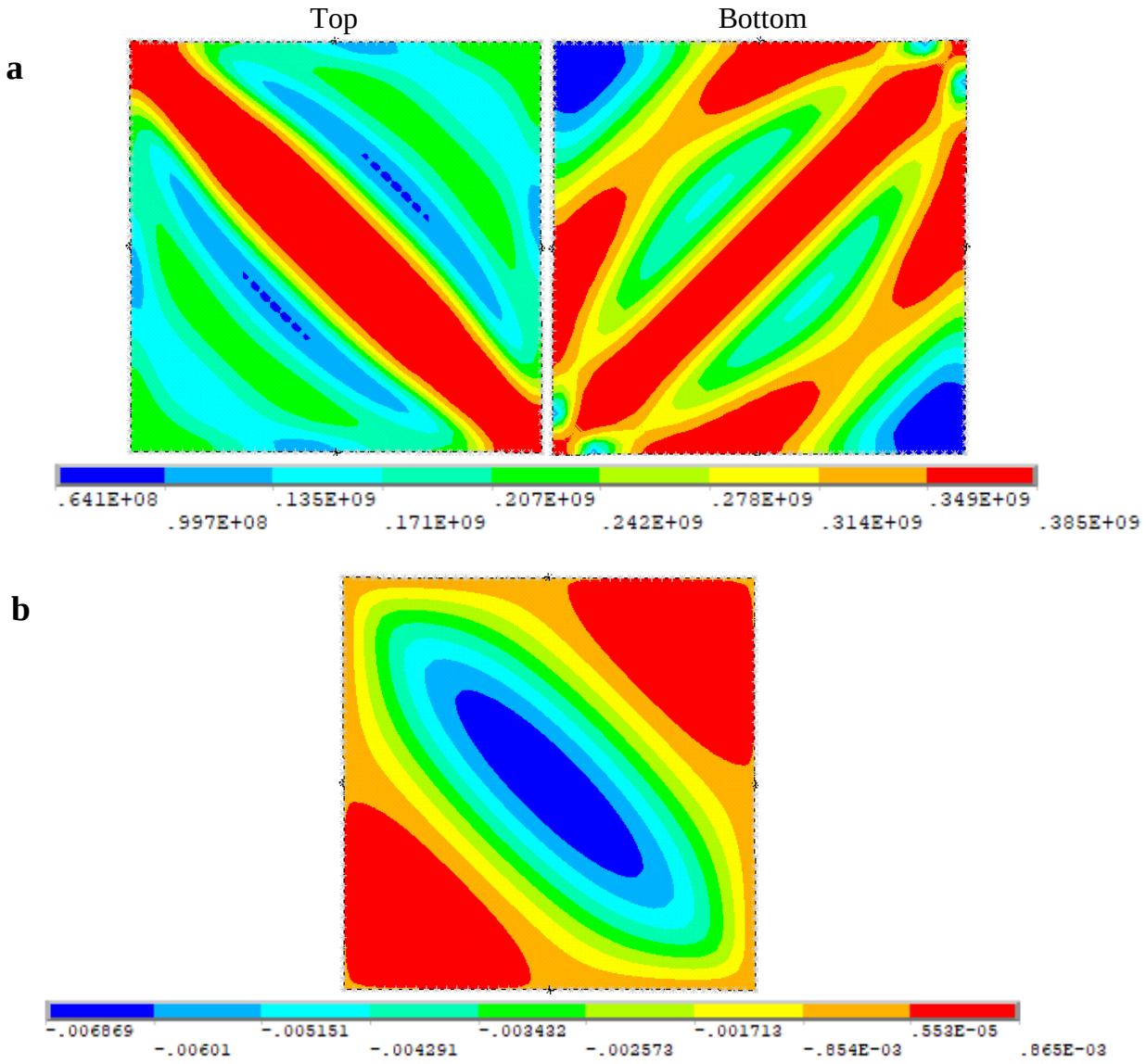

Figure 3: (**a**) Von Mises stress contours in Pa at the top and bottom surfaces and (**b**) out-of-plane deflection contour in m corresponding to the postbuckling collapse of a square aluminum plate under pure shear with*b/t* =106.7

Figure 4 (a) illustrates the von Mises stress contours at the top and bottom surfaces of the plate with *b/t* = 213.3 at the end of its postbuckling path, which corresponds to the predicted point of secondary buckling. A limited spread of plasticity can be observed at the two corners of the plate.In this case of slenderness ratiothe secondary buckling precedes clearly the collapse of the plate due to material yielding. The out-of-plane deflections corresponding to the secondary buckling point of this plate are presented in Figure 4 (b), where the formation of one symmetric large buckle is observed. The deflection amplitude in this case is greater in comparison with that of thethickest plate of Figure 3 (b).

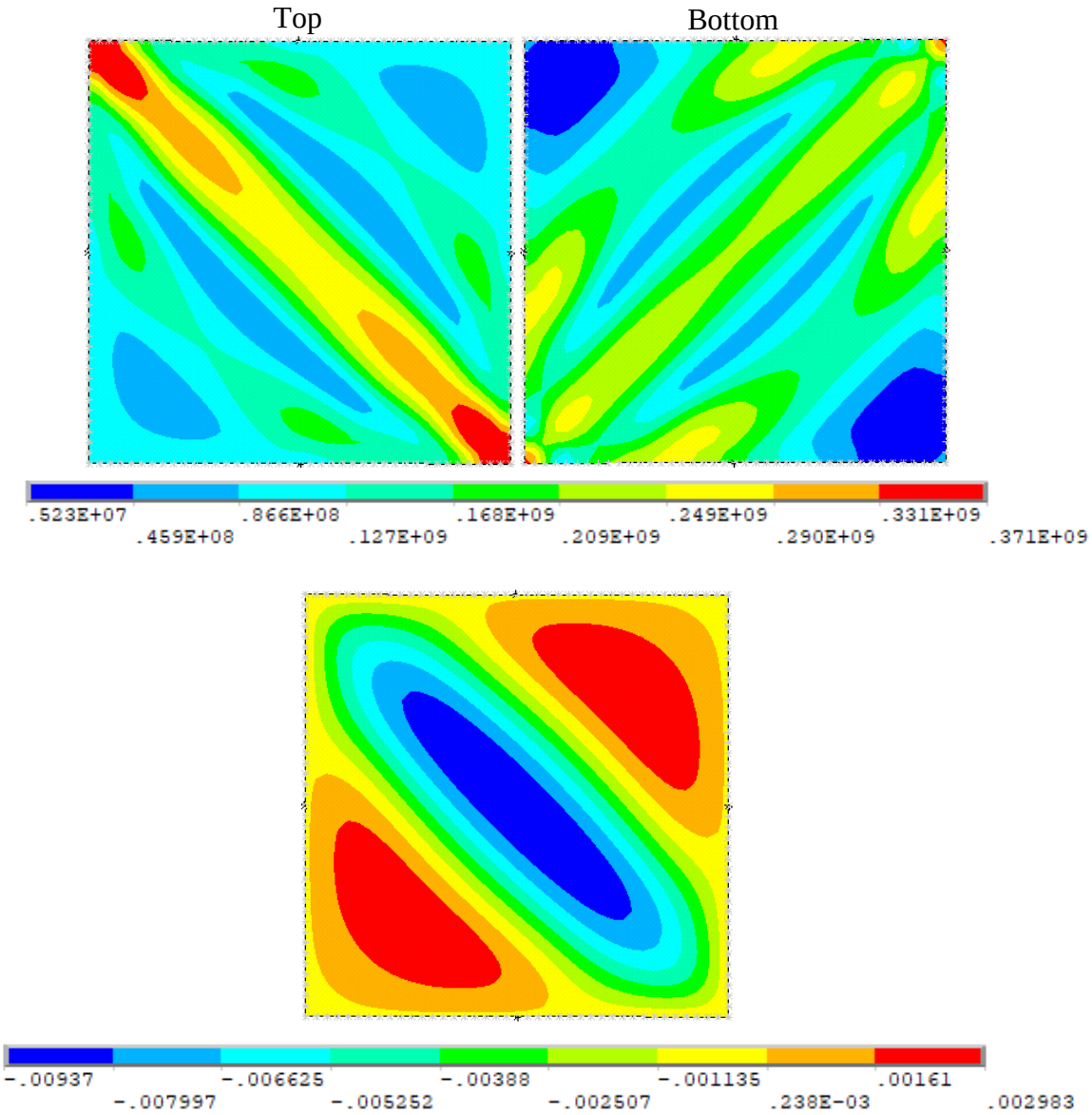

Figure 4: (**a**) Von Mises stress contours in Pa at the top and bottom surfaces and (**b**) out-of-plane deflection contourin m corresponding to the critical pre-secondary-buckling equilibrium state of a square aluminum plate under pure shear with b/t = 213.3

The von Mises stress contours at the top and bottom surfaces of the plate with the greatest slenderness ratio are depicted in Figure 5 (a) at the end of its postbuckling path which also coincides with thepredicted point of secondary buckling. In this case the postbuckling path is completely elastic, since there is not any yielding of aluminum. Figure 5 (b) illustrates the magnitude of the out-of-plane deflections of the plate with slenderness ratio = 426.7, and thedeformation mode is similar to that of Figure 4 (b).

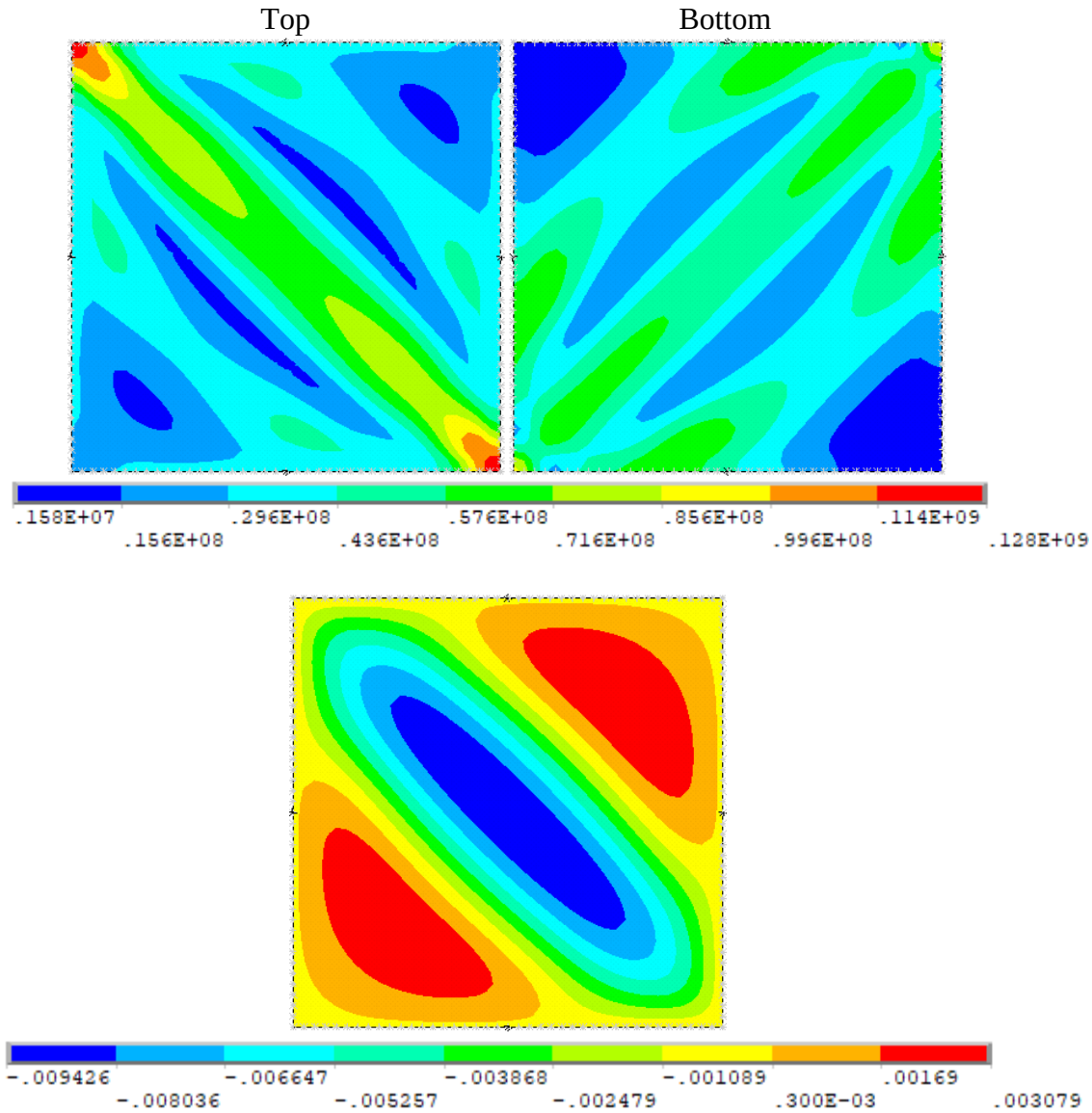

Figure 5: (**a**) Von Mises stress contours in Pa at the top and bottom surfaces and (**b**) out-of-plane deflection contourin m corresponding to the critical pre-secondary-buckling equilibrium state of a square aluminum plate under pure shear with b/t = 426.7

6 CONCUSIONS

- This article deals with the investigation of the postbuckling failure mechanism of aluminum square plates subjected to shearing stresses, taking into account yielding and secondary buckling. A novel FEM procedure is proposed in order to locate the secondary buckling point. This procedure is not limited to the specific problem since it does not depend on the geometry, the loading and the bc of the structure. It is therefore applicable to thin-walled plate and shell structures when secondary buckling phenomena are likely to occur. Load-deflection amplitude curves along with von Mises stress contours have been used in order to predict the postbuckling reserve, the load-carrying capacity of the plates and the spread of plasticity.

- It is found that the primary and secondarybuckling of the analyzed aluminum square simply supported plates under pure shear is strongly affected by the slenderness ratio. As their slenderness ratio decreases, the primary and secondary buckling loads increase.
- It is also found that variations of the slenderness ratio can affect significantly the failure mechanism of the plate, since they can alter the order of first occurrence of the following phenomena as the loading increases: onset of yielding, secondary buckling, collapse of the shear panels.
- For relatively low slenderness ratio, the plate collapses due to the formation of a diagonal yield line. As the plate becomes more slender secondary buckling precedes the onset of yielding.
- The presented study will help aerospace engineers and researchers, investigating the buckling strength of isotropic plates, to evaluate, understand and take advantage of their buckling and postbuckling response.

REFERENCES

[1] Cerini, M. and Falzon, B.G. Use of arc-length method for capturing mode jumping in postbuckling aerostructures. *AIAA J.* (2005) **43**:681-689.

[2] Nakamura, T. and Uetani, K. The secondary buckling and post-secondary-buckling behaviours of rectangular plates. *Int. J. Mech. Sci.* (1979) **21**:265-286.

[3] ANSYS. *Structural Analysis Guide*. ANSYS Inc. (2014).

[4] Yaghoubi, A.S and Liaw, B. Effect of lay-up orientation on ballistic impact behaviors of GLARE 5 FML beams. *Int. J. Impact Eng.* (2013) **54**:138-148.

[5] Fatt, M.S.H., Lin, C., Revilock Jr., D.M. and Hopkins, D.A. Ballistic impact of GLARE^{TM} fiber-metal laminates. *Comp. Struct.*(2003) **61**:73-88.

[6] Bikakis, G.S.E., Kalfountzos, C.D. and Theotokoglou, E.E. Elastic buckling response of rectangular GLARE fiber-metal laminates subjected to shearing stresses. *Aerosp. Sci. Technol.* (2019) **87:**110-118.

[7] Timoshenko, S.P. and Gere, J.M. *Theory of elastic stability.* 2nd ed. McGraw Hill, (1961).

[8] Stein, M. and Neff, J. Buckling stresses of simply supported rectangular flat plates in shear. *NACA* (1947) Technical Note No. **1222**.

[9] Alinia, M.M., Habashi, H.R. and Khorram, A. Nonlinearity in the postbuckling behaviour of thin steel shear panels. *Thin-Walled Struct.* (2009) **47**:412-420.

[10] Stein, M. Postbuckling of eccentric open-section stiffened composite panels. In: *AIAA 29th structures, structural dynamics and materials conference*, Williamsburg, VA, USA, 18-28 April 1998, paper no. **88-2215**, pp. 57-61.